E. POSTEK*, R.B. PĘCHERSKI*, Z. NOWAK*#

PERIDYNAMIC SIMULATION OF CRUSHING PROCESSES IN COPPER OPEN-CELL FOAM

In the last 20 years, a new meshless computational method has been developed that is called peridynamics. The method is based on the parallelized code. The subject of the study is the deformation of open-cell copper foams under dynamic compression. The computational model of virtual cellular material is considered. The skeleton structure of such a virtual cellular material can be rescaled according to requirements. The material of the skeleton is assumed as the oxygen free high conductivity (OFHC) copper. The OFHC copper powder can be applied in additive manufacturing to produce the open-cell multifunctional structures, e.g., crush resistant heat exchangers, heat capacitors, etc. In considered peridynamic computations the foam skeleton is described with the use of an elastic-plastic model with isotropic hardening. The dynamic process of compression and crushing with different impact velocities is simulated.

Keywords: virtual cellular material, metallic foams, OFHC copper, elastic-plastic model, numerical methods, peridynamics, crushing process

1. Introduction

Peridynamics is a new and rapidly developing meshless computational method. The method extending rapidly over many branches of mechanics of solids is based on the parallelized code. Its particular feature is the non-locality. Several non-local methods are already developed. A state-of-the-art of the methodologies is given in Voyiadjis [20]. There are described applications of gradient plasticity methods, fractional methods, micropolar plasticity methods, combinations of molecular dynamics and finite element method and peridynamics. Particular developments of the fractional methods are given in Sumelka [21,22]. The direct predecessors of the peridynamics are the non-local descriptions of crystal mechanics, see Rogula [17], Kunin [18]. The non-local methods were generalized to describe coupled problems in Eringen [19].

The peridynamics was started to develop by Silling [1] and examples of brittle damage simulations under impact were given in Silling and Ascari [2]. Theoretical foundations of peridynamic states vis-à-vis constitutive modelling were discussed in Silling et al. [3]. The subject of the study presented in the paper is the deformation of open-cell copper foams under dynamic compression. The skeleton structure of the cellular material is considered as virtual material with topology generated by tomograms of polyurethane foams, Stręk [4] obtained according to the reconstruction methodology presented in Nowak et al. [5] and applied for metallic foams by Pęcherski et al. [6]. The skeleton material is assumed as the oxygen free high conductivity OFHC copper

and can be rescaled according to requirements. The OFHC copper powder can be applied in additive manufacturing to produce the open-cell multifunctional structures, e.g., crush resistant heat exchangers, heat capacitors, etc. In the presented peridynamic computations the foam skeleton is described with use of elastic-plastic model, with isotropic hardening. The dynamic process of compression and crushing during impact is simulated. In [6], the elastic-viscoplastic model with Huber-Mises-Hencky quasi-static yield criterion was used. The experimental data of the strain-rate dependency of yield strength reveal the plateau within the range of strain-rates between 10^{-4} s^{-1} and 10^{3} s^{-1} of rather small influence of strain-rate with the rapid growth of yield limit for higher strain-rates, cf. Fig. 7 in [6]. Such a behaviour is characteristic for fcc metals, and in particular for copper. Therefore, in the present paper elastic-plastic rate independent model is assumed to simplify the peridynamic simulations of crushing processes and reduce the computational costs.

2. Problem statement

The elastic-plastic model in the peridynamic theory is defined in similar form as in the continuous model in the classical mechanics Refs. [7,8] but with a dependence on peridynamic states Mitchell [9].

In Fig. 1, the x and Q are points in the undeformed body. It defines a bond, $\xi = Q - x$. A reference state X is a function that acts on a bond, $X(\xi)$. In analogy to the reference state, the

---

* INSTITUTE OF FUNDAMENTAL TECHNOLOGICAL RESEARCH, POLISH ACADEMY OF SCIENCES, 5B A. PAWIŃSKIEGO STR., 02-106 WARSZAWA, POLAND
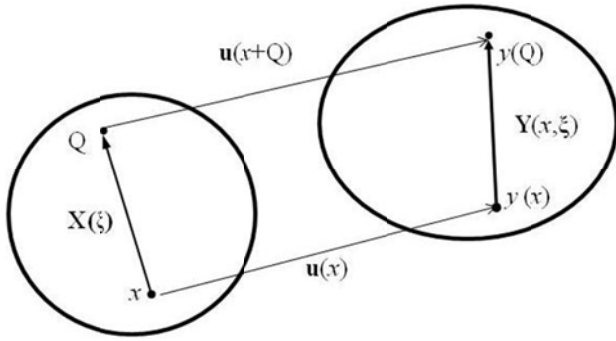
\# Corresponding author znowak@ippt.pan.pl

Fig. 1. Deformation state of a body

deformation state depends on the new position of the coordinate x in the deformed configuration $y(x)$) as follows, $Y(x,\xi) = y(x+\xi) - y(x)$ that yields $Y(x,\xi) = y(Q) - y(x)$. The displacement state $U(x,\xi) = u(x+\xi) - u(\xi)$ that yields $U(x,\xi) = u(Q) - u(x)$. Following Fig. 1, the scalar extension state $e(Y)$ is given as follows:

$$e(Y) = |Y| - |X| \qquad (1)$$

The scalar extension state can be decomposed into its spherical e^i and deviatoric e^d parts:

$$e = e^i + e^d \qquad (2)$$

The elastic force state $t(Y)$ is given in the form analogous to standard stress strain relation being the sum of the spherical and deviatoric parts as follows:

$$t(Y) = \frac{3k\theta}{m}\omega\underline{x} + \alpha\omega e^d \qquad (3)$$

where k is the bulk modulus, θ is the dilatation, m is the weighted volume, ω is the influence function, $\underline{x} = |\xi|$ is the basic scalar state, α is the coefficient related to the shear modulus $\alpha = (15\mu)/m$ where μ is the shear modulus.

Further set of relations has the structure similar to the classical theory of plasticity. The additive decomposition of the deviatoric extension state e^d into elastic state e^{de} and plastic state e^{dp} is of the form:

$$e^d = e^{de} + e^{dp} \qquad (4)$$

Elastic force state relation considering the relation (3) and (4) reads:

$$t(Y) = \frac{3k\theta}{m}\omega\underline{x} + \alpha\omega\left(e^d - e^{dp}\right) \qquad (5)$$

Yielding condition where ψ_o is the yielding limit and ψ is a function of the deviatoric state, reads:

$$f\left(t^d\right) = \psi\left(t^d\right) - \psi_o \leq 0, \text{ where } \psi\left(t^d\right) = \frac{\left\|t^d\right\|^2}{2} \qquad (6)$$

Flow rule where the dot (·) denotes the rate of the plastic state e^{dp} and λ is the consistency parameter reads:

$$\dot{e}^{dp} = \lambda\nabla^d\psi \qquad (7)$$

Kuhn-Tucker conditions (loading and unloading) are as follows:

$$\lambda \geq 0, \quad f\left(t^d\right) \leq 0, \quad \lambda f\left(t^d\right) = 0 \qquad (8)$$

Consistency condition is given below:

$$\lambda\dot{f}(t^d) = 0 \qquad (9)$$

Given the set of relations above allows for the further derivation of the relationships for specific yield functions.

3. Numerical model and material properties

The metallic foam sample is a cube of dimensions 0.0025×0.0025×0.0025 m of the following material properties that are collected in Table 1.

TABLE 1

Copper material properties

Parameters	Values and Units
Young's modulus	110 GPa
Poisson's ratio	0.296
Yield limit	50.0 MPa
Hardening modulus	50.0E+04 Pa
Density	8960 kg/m³

We assume elastic-plastic material with isotropic hardening. The geometry of the foam is obtained from CT scans that are converted into finite element mesh. The CT scans are transformed into a basic tetrahedral mesh with ScanIP+FE [10]. Further processing of the initial mesh is done with GiD [11] and GMSH [12] programs. GiD program is used for visualisation of the results. We use Peridigm program [13] for the calculations.

4. Numerical results

4.1. Numerical model for quasi-static simulations

The numerical model is given in Fig. 2. The structure is discretised with 585897 points. The axonometric and side views are shown in Fig. 2(a) and Fig. 2(b), respectively. In Fig. 2(b), a detail A is marked that is enlarged in Fig. 2(c). There is presented a piece of the complex discretisation.

The structure is loaded with monotonically growing displacement of the top of the sample. The bottom of the sample is constrained against the z-axis direction. The maximum prescribed displacement is 0.222E-05 m against z-axis direction. It stands for 8.8% of the height of the sample. It is applied in total 450 equal steps. Each time step requires between two and four equilibrium iterations. It is used a pool of 960 processes. We used processors of CRAY XC40 system, Intel Xeon E5-2690 V2 consisting of 24 cores with hyperthreading option. The total calculation "wall-clock" time was 14 hours 45 minutes.
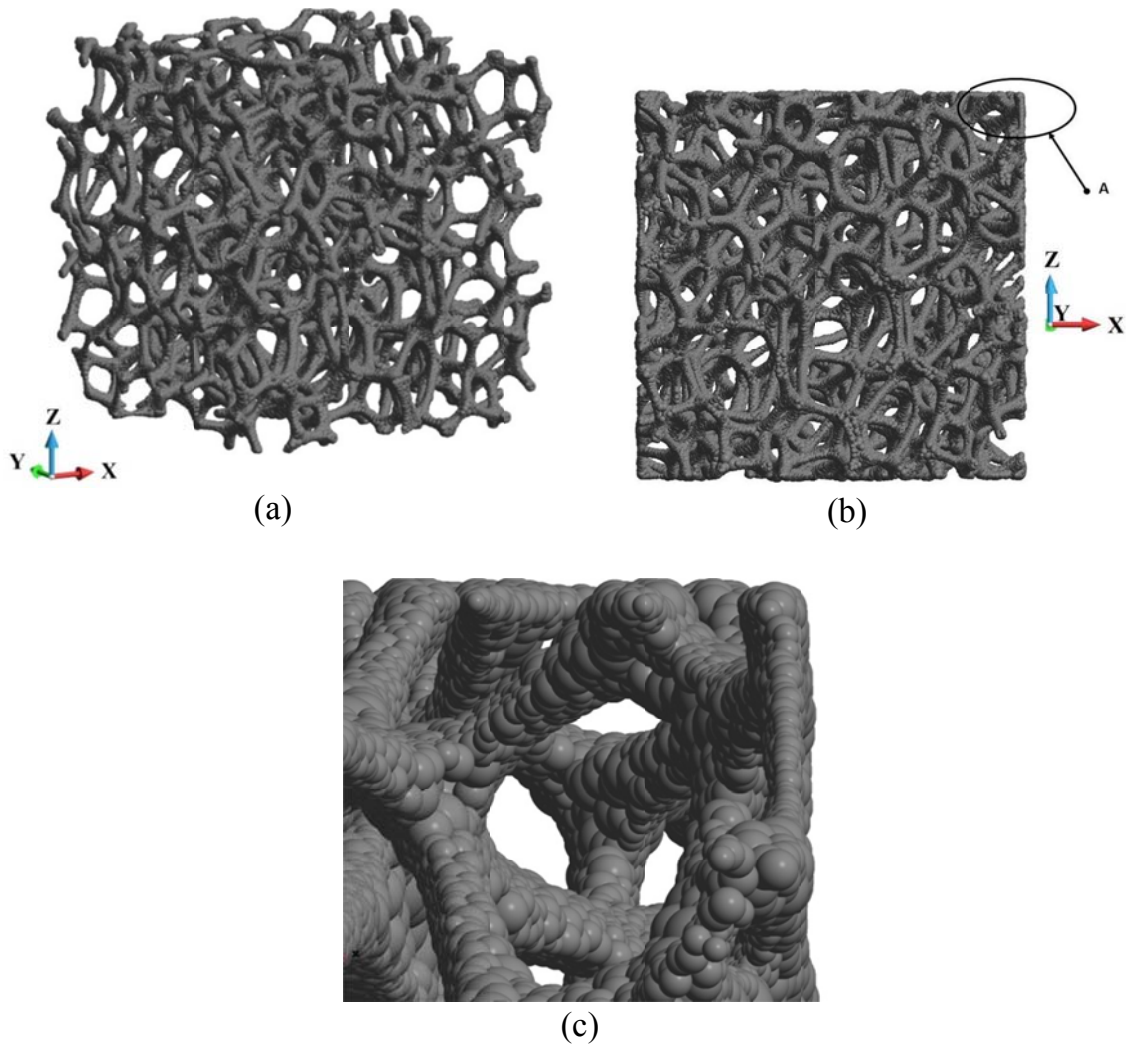
Fig. 2. Particle discretised foam; (a) axonometric view; (b) side view with marked enlarged region A; (c) enlarged region A

The displacement fields are depicted in Fig. 3. Firstly we present the displacement field at the beginning of the loading process when plastic strains start to appear, and secondly the displacement field at the end of the process, Fig. 3(a) and Fig. 3(b), respectively. The prescribed displacement for the pseudo-time 0.002 is 0.50E-06 m and for the pseudo-time 0.009 is the maximum displacement. The displacement fields are qualitatively different. At the beginning of the process, we observe a classical
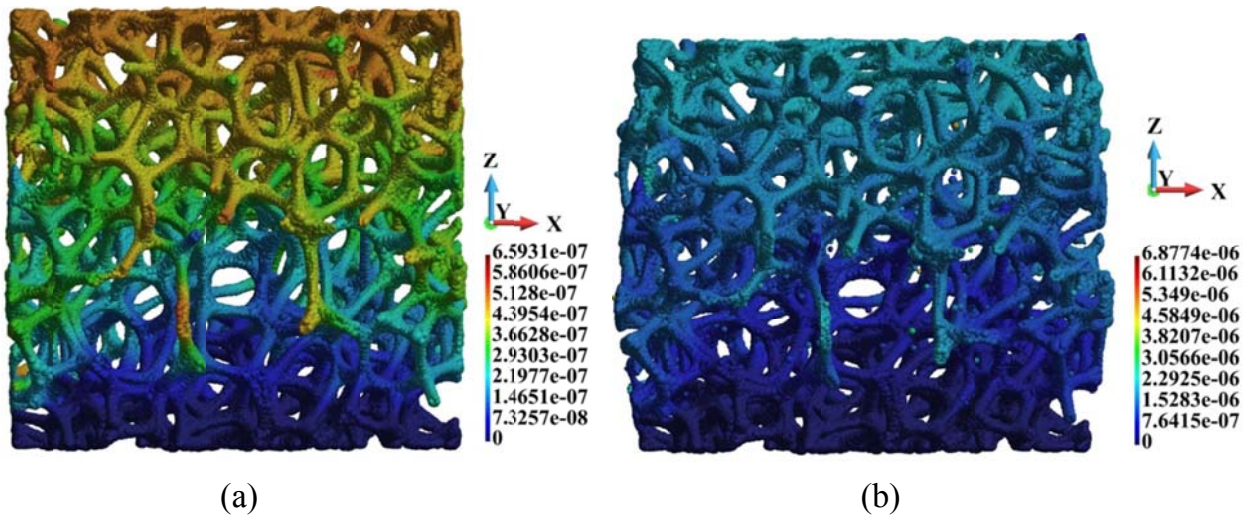

Fig. 3. Displacement fields (m); a) pseudo-time 0.002; b) pseudo-time 0.009

arching under compression, Janas et al. [14], even though the shape of the structure is very complex. Further, when the process advances, the shape of the sample becomes barrel-like.

Huber-Mises-Hencky (HMH) stress fields at the beginning and the end of the loading process are shown in Fig. 4 and Fig. 5, respectively. We observe that HMH stress reaches yield in several branches along the entire height of the sample, Fig. 4(a). In Fig. 4(b), an enhancement of the HMH stress in the range of 0.0 MPa to 16.0 MPa is given. The presentation of the stress distribution in the mentioned range allows us to confirm that the stress distribution is relatively uniform in the sample. When analysing Fig. 5(a) and Fig. 5(b) we find that the maximum HMH stress is slightly above the initial yielding stress, namely 50.014 MPa. The small stress increase is due to the small hardening modulus. We observe the stress that is about the initial yielding limit and above at the top of the sample and mostly in the inner parts of the sample. In the Fig. 5(b) where we show only the points in which the stress is higher than 40 MPa, we find that mostly the branches of the foam posses such stress, that are positioned along the z-direction and mostly not on the edges.

Further on, we observe equivalent plastic strain distribution. In Fig. 6, we find the maximum equivalent strain at the beginning phase of the loading process. The location of the maximum equivalent plastic strain is given in Fig. 6(a). We note that the maximum equivalent plastic strain is at the tip of the narrowing branch of the foam, Fig. 6(c). We present only points where the equivalent plastic strain is greater than zero using a logarithmic scale, Fig. 6(b). The points are located close to the half of the height of the sample and at its top.

Finally, we present a collection of points where equivalent plastic strain appears, Fig. 7. In the interior of the sample, we find the most of the points, Fig. 7(a). We find the points forming entire horizontal branches at the top of the sample, Fig. 7(b). Also, we observe most of the points at the half of the height of the sample, Fig. 7(c).
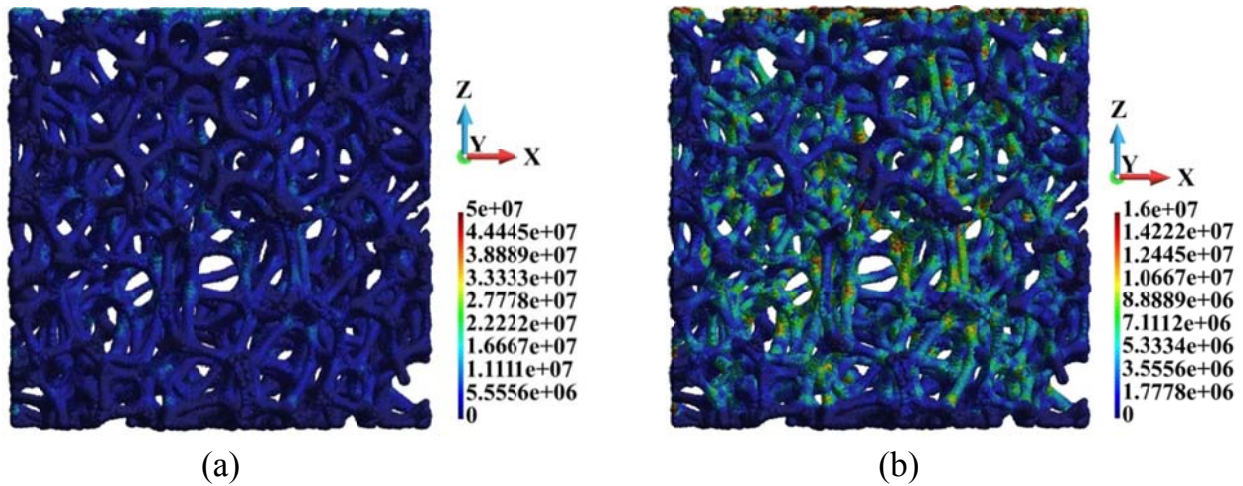

(a)

(b)

Fig. 4. HMH stress fields (Pa), pseudo-time 0.002; a) side view; b) enhanced range 0.0 to 16 MPa
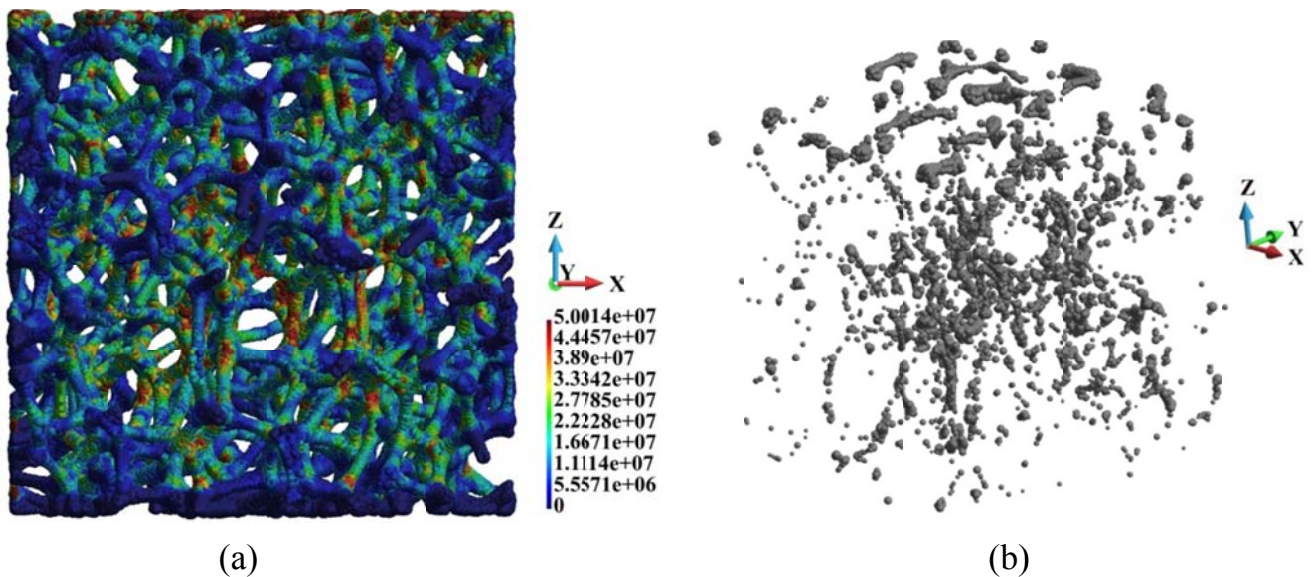

(a)

(b)

Fig. 5. HMH stress fields (Pa), pseudo-time 0.009; a) side view; b) axonometric view of the points collection where HMH stress is higher than 40 MPa
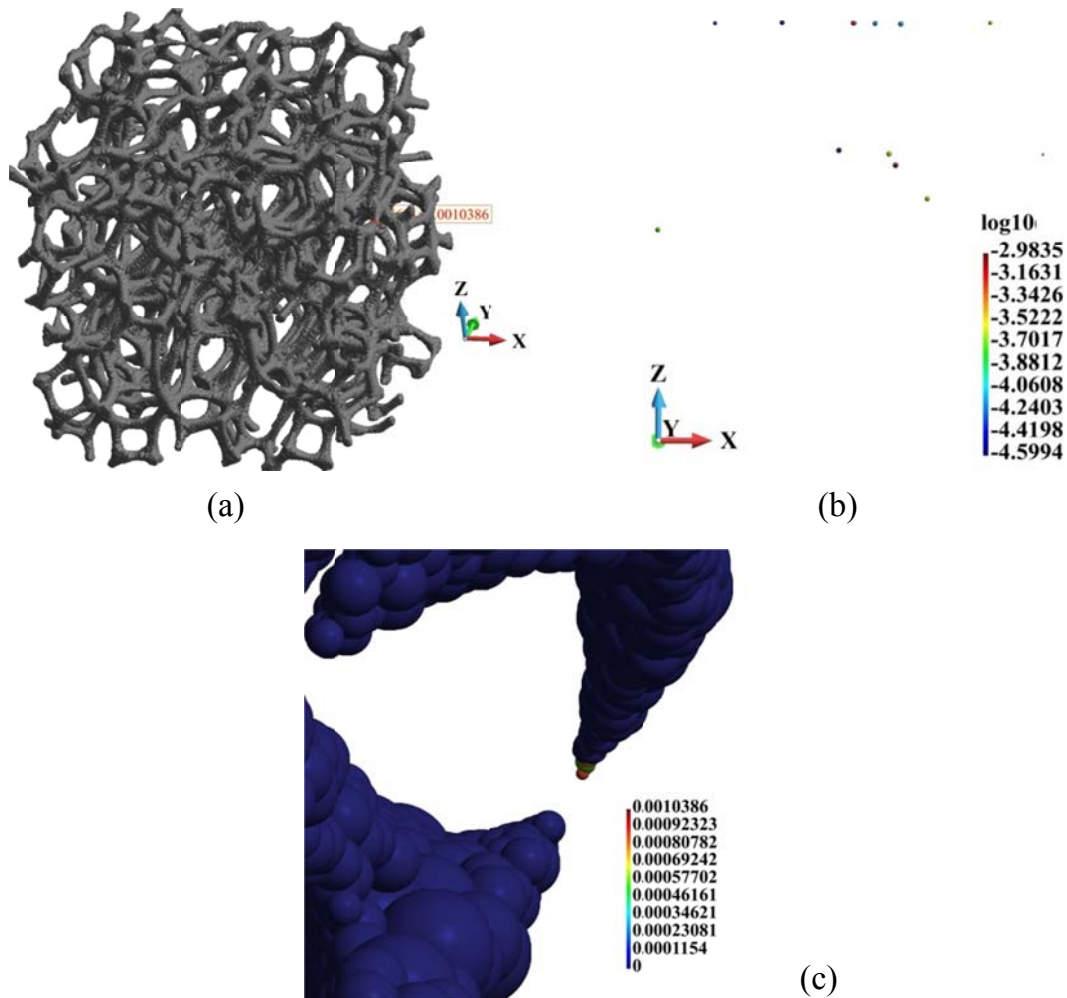
(a)

(b)

(c)

Fig. 6. Equivalent plastic strain at pseudo-time 0.002; a) position of the highest equivalent plastic strain b) points where plastic strain appears; c) equivalent plastic strain at the tip of a branch

4.2. Numerical model for impact calculations

The further analysis concerns the impact of the sample of the foam against stiff but not rigid surface of a block. The scheme of the system is given in Fig. 9(a). The sample hits the block with initial velocity V of 20 m/s. The impact process is followed up to 10.0E-07 s. We use finer discretisation than in the static case. The foam is discretised with 2651427 points. Besides, the base is discretised with 1600000 points. The dimensions of the base are 0.0035×0.0035×0.001 m. The material is ideally elastic. The material properties of the base are given in Table 2.

TABLE 2

Material parameters of the base

Parameters	Values and Units
Young's modulus	210 GPa
Poisson's ratio	0.296
Density	8960 kg/m^3

The shape of the sample is given in Fig. 9(b). We note a qualitative difference of the shape after impact and the quasi-

static compression, Fig. 3(b). In the case of the impact, a flattening of the attacking part of the sample appears while in the static case, the shape of the sample resembles a barrel. The maximum z-displacement of the nodes at the top of the sample is 0.1975E-04 m that stands for 8.0% of the height of the sample.

The general contact conditions between all external surfaces of the foam are applied that means the self-contact as well. The contact algorithm is implemented into Peridigm in its penalty version method. The model is valid for explicit time integration. It is a contact between all facets into which a sphere surrounding a point is converted, Fig. 8.

The HMH stress distribution is shown in Fig. 10. We note that the higher stress region reaches half of the sample relatively uniformly, Fig. 10(a). It is in contrast to the static case where the stress that is close to yielding limit is distributed rather uniformly along the z-axis in the entire sample, Fig. 5(a) and Fig. 5(b).

Equivalent plastic strain distribution is given in Fig. 11. The plastic strains are concentrated at the lower part of the sample, Fig. 11(a), namely, in the neighbourhood of the flattened part of the sample, Fig. 9(a). We find that plastic strains are concentrated strongly since entire branches of the foam are affected,
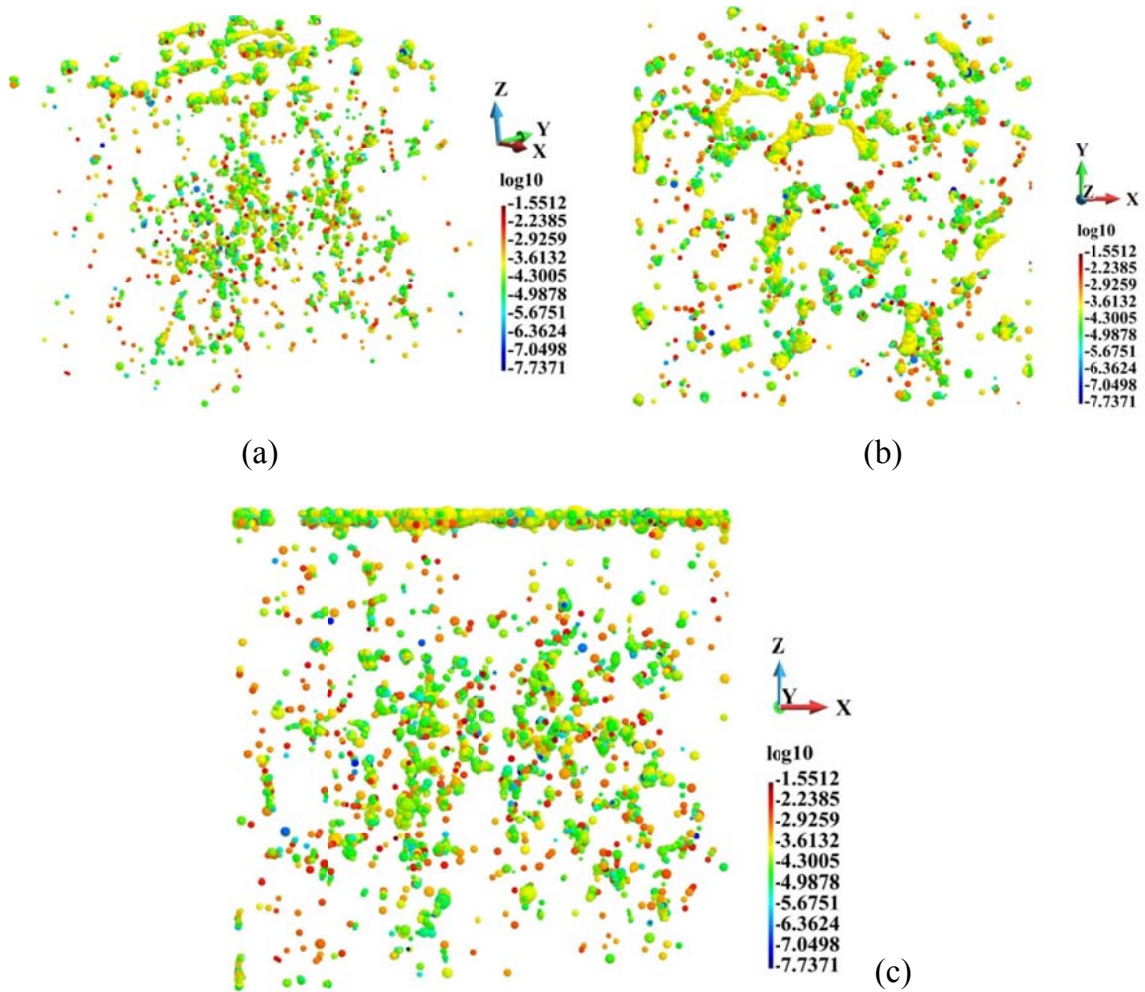
1608

Fig. 7. Equivalent plastic strain at pseudo-time 0.009; a) axonometric view; b) top view; c) side view
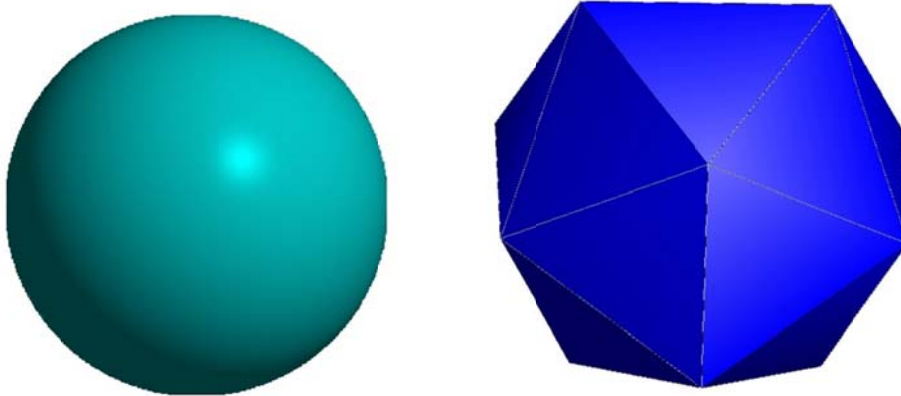

Fig. 8. Conversion of a sphere surrounding a point into an icosahedron for contact detection

Fig. 11(b). Again, we find a qualitative difference between the quasi-static case and the impact. Namely, in the quasi-static case, when the process is advanced plastic strains appear in practically in all branches, Fig. 7(a) and Fig. 7(b). In the case of impact, plastic strains appear close to the hitting part of the sample. In this case, the same processor and the same number of processes were used. We use explicit time integration technique. The time step is 1.97555E-09 s constant in the entire time domain. The total calculation "wall-clock" time was 2.5 hours.

5. Summary

The behaviour of a sample of a copper foam was investigated. The models of the sample for quasi-static compression and impact against a solid block were created. The similar shortening of the sample in both cases, namely, 8% of the sample was assumed. The following conclusions can be collected:

• the displacement fields in the case of quasi-static and impact cases are qualitatively different, namely, in the quasi-static
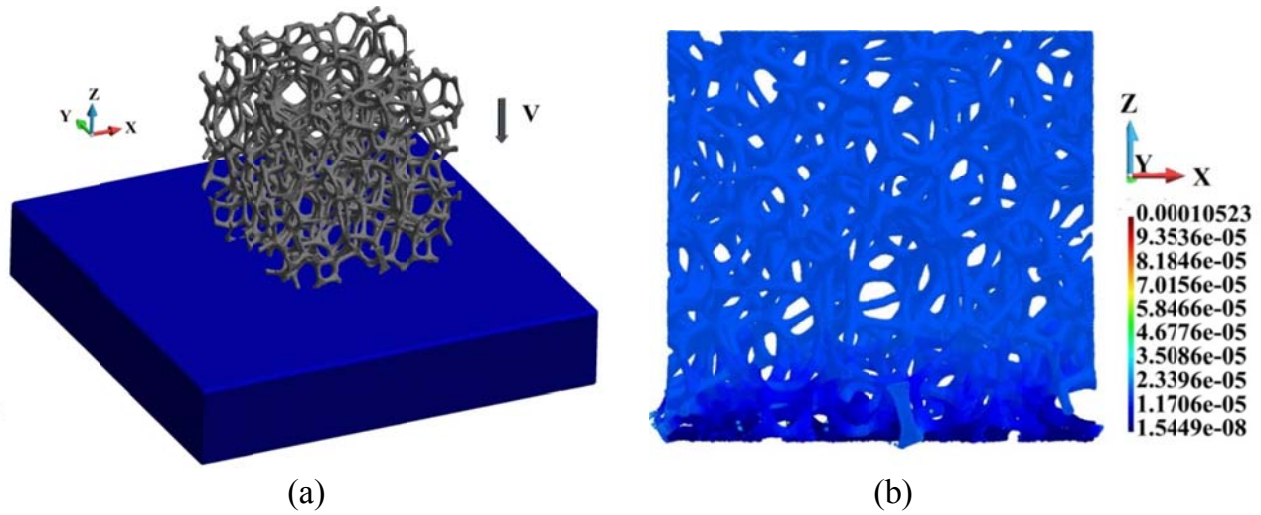
Fig. 9. Scheme of the structure (a) displacement (m) field (scaled 5 times) and shape of the structure at the end of the observed time interval (b)
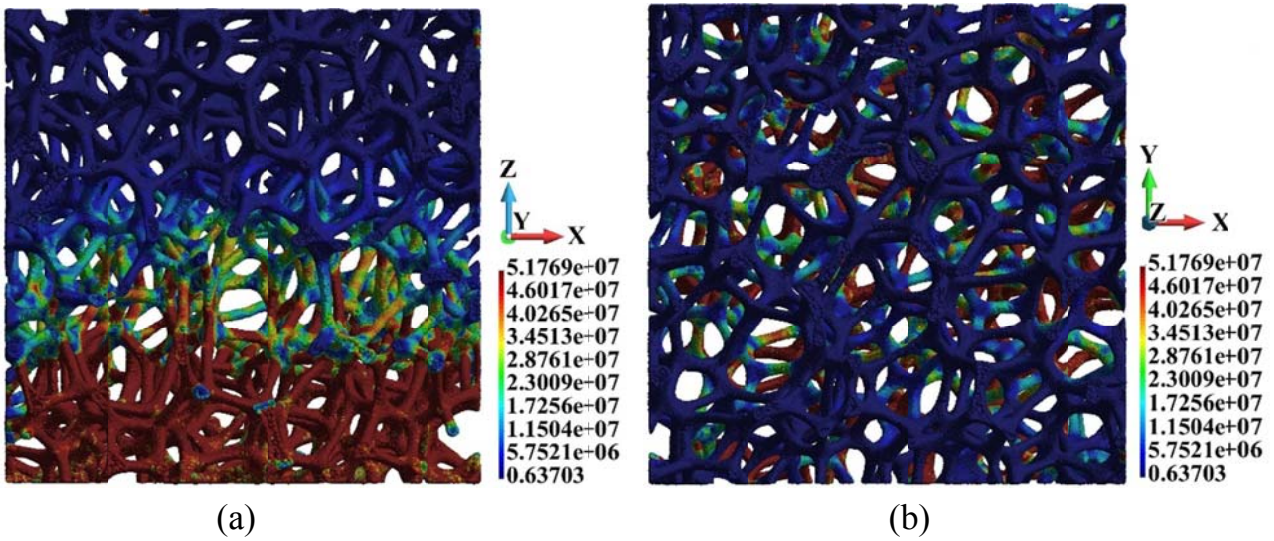

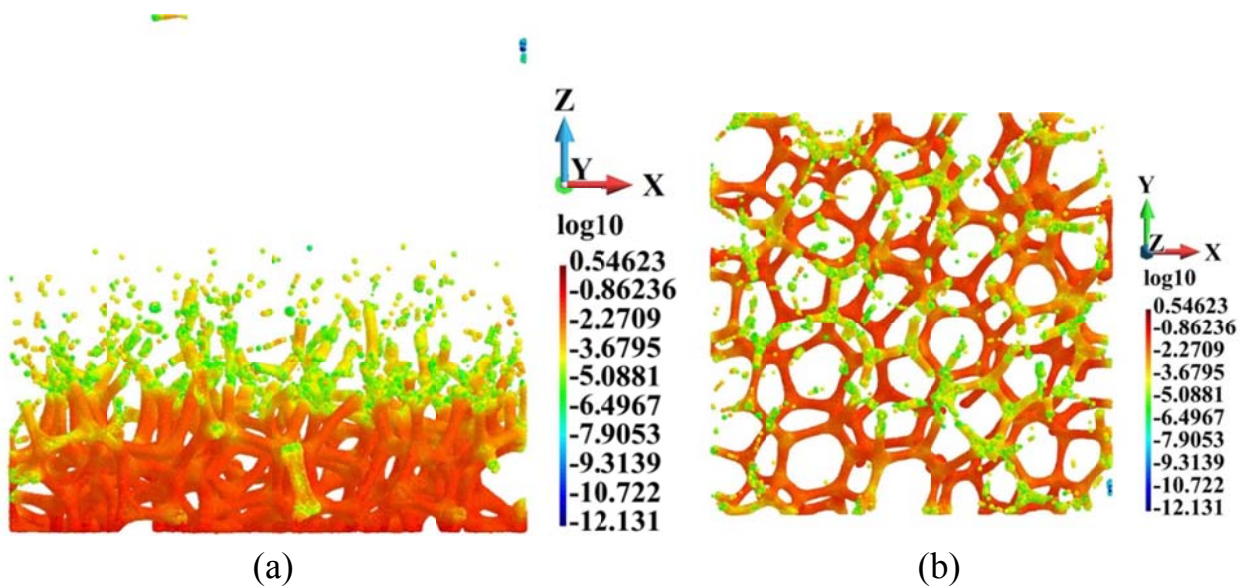Fig. 10. HMH stress at time 10E-07 s; (a) side view; (b) top view

Fig. 11. Equivalent plastic strain at time 10E-07 s; (a) side view; (b) top view

case the deformation of the sample is of barrel-like shape while in the impact case a stamp-like shape is formed,

- the HMH stress fields in the quasi-static and impact cases are qualitatively different, namely, in the quasi-static case the HMH stress is concentrated quite uniformly in the foam branches that are closer to the middle of the sample along the z-axis while in the impact case the higher HMH stress field region reaches half of the sample starting from the base,

- the equivalent plastic strain fields in the quasi-static and impact cases are qualitatively different, namely, in the quasi-static case the equivalent plastic strain is distributed quite uniformly in the sample, but we have found less points where plastic strains occur in the foam branches close to the bounding surfaces than in the interior of the sample, while in the impact case plastic strains appear in the foam branches close to the attacking surface of the sample, namely in the neighbourhood of the formed stamp, and in the latter case, in the entire branches of plastic strains occur.

Also, the general conclusion concerning the application of the simplified rate independent elastic-plastic model can be underlined. The application of more accurate elastic-viscoplastic model applied in Pęcherski et al. [6] should be implemented for peridynamic simulations of crushing processes of copper open-cell foam, and the computational cost of both approaches mentioned above should be compared. The more sophisticated model of the viscoplastic flow of copper skeleton accounting for micro-shear banding, Pęcherski [15], Nowak et al. [16], can also be implemented in the peridynamic analysis. Further possible developments can be done towards implementation of viscoplastic models following Refs. [23-26]. It is the subject of further studies.

REFERENCES

[1] S.A. Silling, Reformulation of elasticity theory for discontinuities and long-range forces, J. Mech. Phys. Solids **48**, 175 (2000).

[2] S.A. Silling, E. Askari, A mesh free method based on the peridynamic model of solid mechanics, Computers and Structures **83**, 1526-1535 (2005).

[3] S.A. Silling, M. Epton, O. Weckener, J. Xu, E. Askari, Peridynamic states and constitutive modeling, J. Elasticity **88**, 151-184 (2007).

[4] A. Stręk, Production and study of polyether auxetic foam, Mech. Control 29, 78-87 (2010).

[5] M. Nowak, Z. Nowak, R. Pęcherski, M. Potoczek, R. Śliwa, On the reconstruction method of ceramic foam structures and the methodology of Young modulus determination, Arch. Metal. Mater. **58**, 1219-1222 (2013).

[6] R.B. Pęcherski, M. Nowak, Z. Nowak, Virtual metallic foams, applications for dynamic crushing analysis, Int. J. Multiscale Comput. Engng. **15**, 431-442 (2017).

[7] J. Lubliner, Plasticity Theory, Dover Publications (2008).

[8] R. Hill, The Mathematical Theory of Plasticity. Oxford University Press: Oxford (1998) (first edition 1956).

[9] J.A. Mitchell, A nonlocal, ordinary, state-based plasticity model for peridynamics, Sandia report, SAND2011-3166 (2011).

[10] ScanIP+FE, www.simpleware.com/software/scanip, ver. 7.0 (2014).

[11] GiD http://www.gidhome.com/.

[12] GMSH http://gmsh.info/.

[13] Peridigm Users'Guide, M.L. Parks, D.J. Littlewood, J.A. Mitchell, S.A. Silling, Tech. Report SAND2012-7800, Sandia National Laboratories (2012).

[14] M. Janas, J. Sokół-Supel, E. Postek, Arching action in slackened structures, Foundations of Civil and Environmental Engineering **1**, pp. 97-109 (2002).

[15] R.B. Pęcherski, Macroscopic measure of the rate of deformation produced by micro-shear banding, Arch. Mech. **49**, 385-401 (1997).

[16] Z. Nowak, P. Perzyna, R.B. Pęcherski, Description of viscoplastic flow accounting for shear banding, Arch. Metal. Mater. **52**, 217-218 (2007).

[17] D. Rogula, Nonlocal theory of material media, Springer, Wien, New-York (1982).

[18] A. Kunin, Elastic media with microstructure, one dimensional models, Springer, Berlin, Heidelberg, New-York (1982).

[19] A.C. Eringen, Nonlocal continuum field theories, Springer, New-York, Berlin, Heidelberg (2001).

[20] G.Z. Voyiadjis, Handbook if Nonlocal Continuum Mechanics for Materials and Structures, Springer (2019).

[21] W. Sumelka, A note on non-associated Drucker-Prager plastic flow in terms of fractional calculus, Journal of Theoretical and Applied Mechanics **52**, 571-574 (2014).

[22] W. Sumelka, Non-local Kirchhoff-Love plates in terms of fractional calculus, Archives of Civil and Mechanical Engineering **15**, 231-242 (2015).

[23] J. Litoński, Plastic flow of a tube under adiabatic torsion, Bulletin de l'Academie Polonaise des Sciences **25**, 7-17 (1977).

[24] R.C. Batra, L. Chen, Effect of viscoplastic relations on the instability strain, shear band initiation strain, the strain corresponding to the minimum shear band spacing, and the band width in a thermoviscoplastic material, International Journal of Plasticity **17**, 1465-1489 (2001).

[25] P. Perzyna, Fundamental problems in viscoplasticity, Adv. Appl. Mech. **9**, 243-377 (1966).

[26] W. Sumelka, T. Łodygowski, The influence of the initial microdamage anisotropy on macrodamage mode during extremely fast thermomechanical processes, Archive of Applied Mechanics **81** (12), 1973-1992 (2011).